Free Radical Research, February 2011; 45(2): 211–220

Stage-specific roles of *fibulin*-5 during oxidative stress-induced renal carcinogenesis in rats

HIROKI OHARA[1,2], SHINYA AKATSUKA[1], HIROTAKA NAGAI[1,2], YU-TING LIU[2], LI JIANG[1], YASUMASA OKAZAKI[1], YORIKO YAMASHITA[1], TOMOYUKI NAKAMURA[3] & SHINYA TOYOKUNI[1]

[1]*Department of Pathology and Biological Responses, Graduate School of Medicine, Nagoya University, Showa-ku, Nagoya 466-8550, Japan,* [2]*Department of Pathology and Biology of Diseases, Graduate School of Medicine, Kyoto University, Sakyo-ku, Kyoto 606-8501, Japan, and* [3]*Department of Pharmacology, Kansai Medical University, Osaka 570-8506, Japan*

(Received date: 22 August 2010; In revised form date: 7 September 2010)

Abstract

By using a rat model of renal cell carcinoma (RCC) induced by ferric nitrilotriacetate (Fe-NTA), this study performed genome-wide analysis to identify target genes during carcinogenesis. It screened for genes with decreased expression in RCCs, with simultaneous loss of heterozygosity, eventually to focus on the *fibulin-5* (*fbln5*) gene. Oxidative damage via Fe-NTA markedly increased Fbln5 in the proximal tubules. RCCs presented lower levels of Fbln5. However, a fraction of RCCs presenting pulmonary metastasis revealed significantly higher levels of Fbln5 than those without metastasis, accompanied by immunopositivity of RCC cells and myofibroblast proliferation. Experiments revealed that RCC cell lines showed lower expression of *fbln5* than its non-transformed counterpart NRK52E, but that *fbln5* transfection to RCC cell lines changed neither proliferation nor migration/invasion. The data suggest that Fbln5 plays a role not only in the tissue repair and remodelling after renal tubular oxidative damage but also in RCC metastasis, presumably as a cytokine.

Keywords: *Fibulin-5 (FBLN5), ferric nitrilotriacetate, oxidative damage, renal cell carcinoma, metastasis, myofibroblast*

Abbreviations: *aCGH, array-based comparative genomic hybridization; α-SMA, α-smooth muscle actin; bp, base pairs; DMEM, Dulbecco's modified Eagle's medium; FBLN5, fibulin-5; FBS, foetal bovine serum; Fe-NTA, ferric nitrilotriacetate; LOH, loss of heterozygosity; PCR, polymerase chain reaction; RCC, renal cell carcinoma.*

Introduction

Living cells are constantly exposed to potentially damaging reactive oxygen and nitrogen species. These reactive species are produced either by normal cellular metabolism or by exposure to various xenobiotics, including barbiturates, chlorinated compounds, transitional metal ions and radiation [1,2]. A growing body of evidence has established a link between oxidative damage and carcinogenesis [3–5].

We have developed a rodent model of renal cell carcinoma (RCC) induced by ferric nitrilotriacetate (Fe-NTA; an iron chelate) in order to study the mechanisms of oxidative stress-induced cancer. Intraperitoneal administration of Fe-NTA induces renal proximal tubular damage, a consequence of a Fenton-like reaction that ultimately leads to a high incidence (60–92%) of RCCs in rodents [6–8]. Previous studies revealed that oxidatively modified DNA bases including 8-oxoguanine [9] and a major lipid peroxidation product, 4-hydroxy-2-nonenal [10], along with its modified proteins [11], display increased levels during the early stage of RCC development in

Correspondence: Shinya Toyokuni, MD, PhD, Department of Pathology and Biological Responses, Nagoya University Graduate School of Medicine, 65 Tsurumai-cho, Showa-ku, Nagoya 466-8550, Japan. Tel: +81 52 744 2086. Fax: +81 52 744 2091. Email: toyokuni@med.nagoya-u.ac.jp

ISSN 1071-5762 print/ISSN 1029-2470 online © 2011 Informa UK, Ltd.
DOI: 10.3109/10715762.2010.523702

this rodent cancer model. The characteristic spectrum of DNA mutations detected following repeated intra-peritoneal administration of Fe-NTA include deletions with short homologous sequences at the deletion junctions as well as single nucleotide substitutions at G:C sites [12].

Genetic analysis of Fe-NTA-induced RCCs revealed frequent inactivation of the *CDKN2A* (*p16*^{INK4A}) and *CDKN2B* (*p15*^{INK4B}) tumour suppressor genes as a result of deletions, point mutations or methylation of the promoter region [13]. Furthermore, loss of heterozygosity at this genetic locus occurs specifically and early in carcinogenesis [14]. Recently, Liu et al. [15] reported data demonstrating the activation of a novel β-catenin pathway that occurs as a consequence of amplification and over-expression of the *ptprz1* tyrosine phosphatase in the Fe-NTA-induced RCCs. Notably, this was the first study demonstrating that chronic oxidative stress is a cause of genomic amplification. Alternatively, non-genetic alterations also play a role in Fe-NTA-induced carcinogenesis. Annexin 2 is under the control of the cellular redox status and its persistent over-expression was found to be associated with proliferation and metastasis [16]. Surprisingly, a recent epidemiological study showed that iron reduction by phlebotomy in a supposedly normal population but with peripheral arterial disease was correlated with a significantly decreased cancer risk [17]. However, molecular mechanisms explaining iron-induced tumour formation are not fully elucidated.

In the present study, we performed array-based comparative genomic hybridization (aCGH) and loss of heterozygozity (LOH) analysis to further evaluate chromosomal regions involved in Fe-NTA-induced RCCs. By combining these data with cDNA microarray results, we decided to focus on the *fibulin-5* (*fbln5*) gene. Fibulin-5 is a secretory glycoprotein associated with endothelial adhesion via RGD motif [18] and elastic fibre formation as a Ca^{2+}-dependent elastin binding protein [19,20]. This is indeed a responsible gene for human cutis laxa [21] and age-related macular degeneration [22]. However, its role in carcinogenesis is still controversial as reviewed [23], and the word 'context-specific' is often used for its function. Namely, *fibulin-5* expression is decreased in human renal cancer, breast cancer, ovarian cancer, colon cancer [24] and lung cancer [25], which might be associated with its function as an endogenous angiogenesis inhibitor [26]. However, it promotes transforming growth factor-β-inducible epithelial mesenchymal transition in breast cancer cells [27]. Here we suggest that *fibulin-5* plays a role not only in the repair and regeneration of oxidative renal tubular damage but also in the metastatic process of Fe-NTA-induced RCCs.

Materials and methods

Fe-NTA-induced renal cell carcinoma model

The Fe-NTA induced-carcinogenesis experiment was performed using male F1 hybrid rats between Fischer 344 and Brown-Norway strains (Charles River, Yokohama, Japan) as previously described [6,8,28]. Twenty-two cases of RCCs were used in this study and histological grade of tumour was determined according to the modified World Health Organization classification as we previously described [8]. Their details are summarized in Table I. The subacute study of repeated injections (5–10 iron mg/kg; 1 or 3 week(s)) was performed with male 6-week-old Wistar rats (Shizuoka Laboratory Animal Center, Shizuoka, Japan) as previously described [8]. The animal experiment committees of the Graduate School of Medicine, Kyoto University and Nagoya University Graduate School of Medicine approved this *in vivo* study.

Loss of heterozygosity (LOH) analysis

LOH analysis was performed as previously described [28]. Briefly, the genomic DNA isolated from the

Table I. Features of 22 cases of Fe-NTA-induced renal cell carcinomas.

Tumour cases	Size (mm)	Metastasis	Invasion	Histological grade	INF
1[a] (FB7-1)[b]	20	None	None	1	beta
2 (FB48-5)	20	None	None	1	alfa
3 (FB32-4)	15	Lung	None	2	beta
4 (FB7-7)	60	Lung	None	2	alfa
5 (BF59-1)	15	Lung	Peritoneal	2	gamma
6 (FB16-6)	30	None	None	2	beta
7 (FB6-4)	20	Pancreas, lung	Peritoneal	3	gamma
8 (FB14-3)	15	None	None	3	alfa
9 (FB14-6)	30	Lung	Peritoneal	3	beta
10 (FB19-3)	15	Lung	None	3	gamma
11 (FB21-2)	40	None	None	3	gamma
12 (FB27-2)	40	None	None	3	beta
13 (FB27-6)	40	Spleen, pancreas, lung	Peritoneal	3	gamma
14 (FB28-7)	30	None	None	3	beta
15 (FB30-5)	60	Lung	Peritoneal	3	gamma
16 (FB32-1)	50	Pancreas, lung	Peritoneal	3	gamma
17 (FB33-7)	70	Lung	Peritoneal	3	gamma
18 (FB37-5)	40	Lung	None	3	gamma
19 (FB45-4)	40	Lung	None	3	gamma
20 (BF51-1)	28	None	None	3	beta
21 (BF56-4)	30	None	None	3	gamma
22 (BF57-5)	25	Lung	Peritoneal	3	gamma

Fe-NTA; ferric nitrilotriacetate; INF, mode of tumour cell infiltration based on reference [8].

[a]Numbers correspond to the tumour numbers in Figures.

[b]Alphabets and numbers in the parentheses mean the tumour sample ID. Refer to text for details.

renal tissue of untreated F1 hybrid rats and RCCs were used for PCR analysis as templates. Primers for each microsatellite marker on the rat chromosome 6 were selected according to the reference rat genome database (http://rgd.mcw.edu/genomescanner/) so that the predicted PCR products would differ in size by at least 8 bp.

Array-based comparative genomic hybridization

Array-based comparative genomic hybridization (aCGH) was performed with an Agilent 185K rat genome CGH microarray chip (Agilent Technologies, Santa Clara, CA) as previously described [15]. Results were analysed with the CGH Analytics Software (Version 3.4).

Gene expression microarray

Gene expression microarray was performed with the Rat Genome 230 2.0 array (Affymetrix Inc., Santa Clara, CA) as previously described (Gene Expression Omnibus accession number GSE7675) [15]. Microarray data were analysed by using GeneChip analysis software (Focus array; Affymetrix).

Quantitative real-time PCR

Total RNA was isolated using Isogen reagent (Nippon Gene Co. Ltd., Tokyo, Japan) according to the manufacturer's protocol. cDNA was synthesized using RNA PCR kit ver. 3.0 (Takara Bio, Shiga, Japan) with random primers. Platinum SYBR Green qPCR SuperMix-UDG kit (Invitrogen, Carlbads, CA) and Real-time PCR system 7300 (Applied Biosystems, Foster City, CA) were used for quantitative real-time PCR analysis. Primer sequences were as follows: *fibulin-5* based on GenBank NM_019153: forward, 5′-TATCAACACGGAAGGAGGGTACA-3′; and reverse, 5′-GCTGGCAGTAACCATAGCGA-3′ (106 bp product); β-*actin* based on NM_031144: forward, 5′-TGTGTTGTCCCTGTATGCCTCTG-3′; and reverse, 5′-ATAGATGGGCACAGTGTGGGTG-3′ (85 bp product).

Western blot analysis

Tissue lysates were prepared by homogenizing in RIPA buffer (20 mM Tris, pH 7.4, 0.1% SDS, 1% Triton X-100, 1% sodium deoxycholate) with a glass homogenizer in the presence of protease inhibitor (Complete Mini; Nippon Roche, Tokyo, Japan). Cell lysates were prepared by directly adding RIPA buffer to cell culture dishes and incubated for 15 min on ice with gentle shaking. The supernatants collected after centrifugation at 15 000 rpm for 15 min were used. The protein concentration was determined with BCA protein reagents (Pierce, Rockford, IL). Western blot analysis was performed as previously described [29]. The anti-mouse/rat-Fibulin-5 rabbit polyclonal antibody (BSYN) [30] and anti-β-actin mouse monoclonal antibody (AC-15, Sigma-Aldrich, Tokyo, Japan) were used at a dilution of 1:500 and 1:2000, respectively. The secondary antibodies were peroxidase-conjugated goat anti-rabbit IgG polyclonal antibody (Dako, Kyoto, Japan) and sheep anti-mouse IgG polyclonal antibody (GE Healthcare, Tokyo, Japan) at a dilution of 1:2000 and 1:5000, respectively. Can Get Signal solution (TOYOBO, Osaka, Japan) containing 0.1% sodium azide was used for dilution of all antibodies.

Immunohistochemical analysis

Tissue samples were fixed in 10% phosphate-buffered formalin and embedded in paraffin. Sections were stained with hematoxylin and eosin and observed under a light microscope. Immunohistochemical analysis was performed with the avidin-biotin complex method as previously described [15]. The anti-Fibulin-5 mouse monoclonal antibody (10A) [31] and anti-α-smooth muscle actin mouse monoclonal antibody (α-SMA; 1A4, Dako) were used at a dilution of 1:50. The secondary antibody was biotinylated rabbit anti-mouse IgG polyclonal antibody (Dako) at a dilution of 1:300.

Cell lines

NRK52E established from a normal rat kidney cell of proximal tubules was purchased from Health Science Research Resources Bank (Osaka, Japan). FRCC001 and FRCC562 cell lines were established from primary Fe-NTA-induced RCCs as previously described [16]. Briefly, tumour tissues were minced in Dulbecco's modified Eagle's medium (DMEM; Nakalai Tesque, Kyoto, Japan) with sterile scissors. The tumour pieces were treated with dispase (Godo Shusei, Matsudo, Chiba, Japan) for 30–60 min at 37°C and supernatant containing cell clumps were obtained after centrifugation at 100 x g. The obtained cells were resuspended in fresh DMEM with 10% foetal bovine serum (FBS) plus MITO serum extender (BD Japan, Tokyo) containing various growth factors and hormones and cultured on dishes coated with collagen type I (Iwaki, Tokyo, Japan). Any remaining fibroblasts were removed by a differential attachment and detachment selection method with trypsin-EDTA and the cells were maintained in DMEM supplemented with 10% FBS, 100 U/ml penicillin, 100 μg/ml streptomycin, 4.5 g/l glucose, 4 mmol/l L-glutamine and 25 mmol/l HEPES at 37°C in a 5% CO_2 atmosphere.

Plasmid constructs and transfection

The coding sequence of rat *Fibulin-5* (GenBank NM_019153) was cloned by RT-PCR using cDNA of rat normal kidney as a substrate with the following primers: forward primer with KpnI site and 'Kozak' consensus sequence, 5'-GGGGTACC(*KpnI*) ACCATGCCAGGATTAAAAAGG-3', and reverse primer with EcoRI site, 5'-CGGAATTC(*EcoRI*)TCA GAACGGATACTGGGACAC-3'. The amplified fragments were digested with *KpnI* and *EcoRI* and cloned into the pcDEF3 expression vector under the control of the human polypeptide chain elongation factor 1α (EF-1α) promoter [32]. The sequence was confirmed with an ABI 3130 Genetic Analyser (Applied Biosystems, Foster City, CA). The NRK52E, FRCC001 and FRCC562 cell lines were stably transfected with an *fbln5*-expressing or control empty vector using the Lipofectamine 2000 reagent (Invitrogen, Carlsbad, CA) according to the manufacturer's protocol and selected with 600–1000 μg/ml (NRK52E and FRCC562) or 200–400 μg/ml (FRCC001) G418 for 2–3 weeks.

Cell proliferation assay

Cells were seeded in 48-well culture plates at a density of 1×10^4 cells/well and grown at least 16 h before initial treatment. After incubation, the Cell Counting Kit-8 (Dojindo Molecular Technologies, Inc., Gaithersburg, MD) was added to each well and cells were incubated for 2 h at 37°C in 5% CO_2 atmosphere. The absorbance was measured with a POWERSCAN 4 microplate reader (DS Pharma Biomedical, Osaka, Japan) at a wavelength of 450 nm with background subtraction at 650 nm. Each experiment was carried out in triplicate.

In vitro migration and invasion assay

Migration and invasion potential of Fe-NTA induced-RCC cell lines were evaluated using 24-well transmembrane chambers (pore size 8 μm, BD Biosciences, Tokyo, Japan) according to the manufacturer's protocol. Briefly, cells in DMEM containing 1% FBS were seeded in matrigel-coated or non-coated upper chambers at a density of 7.5×10^4 (FRCC001) and 1×10^5 (FRCC562) cells/well. As a chemo-attractant, DMEM containing 10% FBS was added in the lower chambers. After incubation for 36 h (FRCC001) or 48 h (FRCC562), cells on the lower surface of the membranes were counted in randomly selected 10 visual fields under a microscope at a magnification of ×100. Each image was captured using ScanScope. Each experiment was carried out in triplicate.

Methylation-specific PCR

Genomic DNA was extracted with DNeasy Blood & Tissue Kits (QIAGEN, Tokyo, Japan) and modified

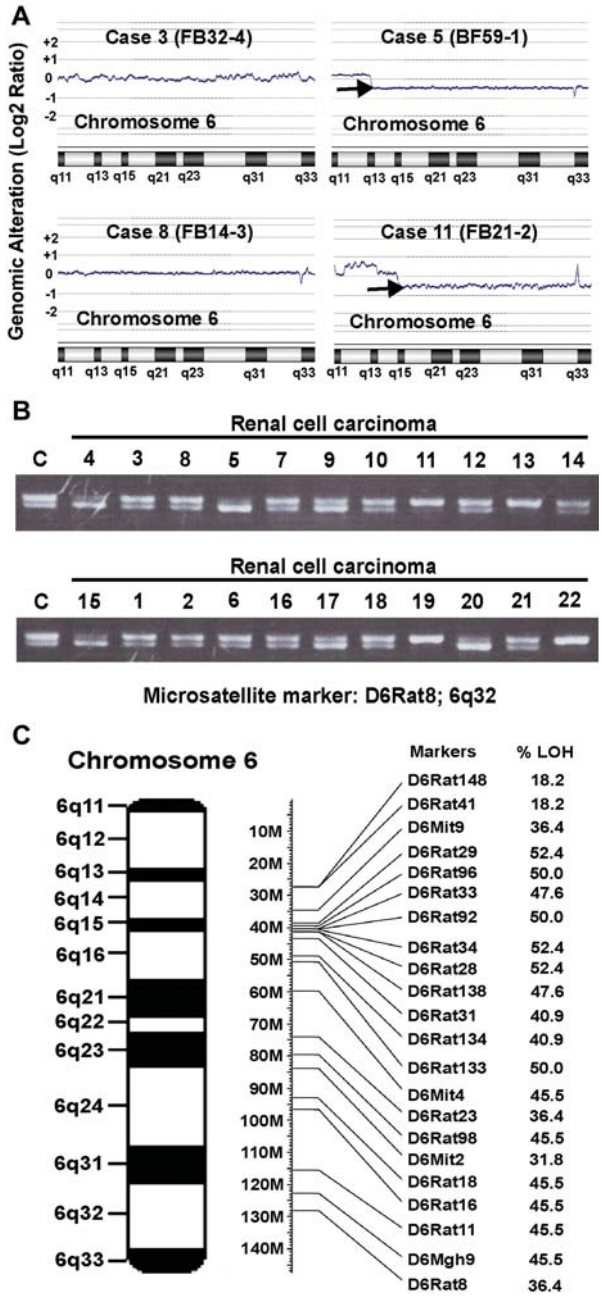

Figure 1. Frequent monoallelic loss of chromosome 6 in Fe-NTA-induced rat renal cell carcinomas (RCCs). (A) Representative results of array-based comparative genomic hybridization analysis of chromosome 6 from genomic DNA of four RCCs. Chromosomal loss or gain was evaluated by comparing the signals obtained from tumour samples to those of normal kidney. The centre-lines indicate the normal 2N state of the genome, while chromosomal loss is defined as lower than the centre line, and chromosomal gain is denoted as higher than the centre line. Arrows indicate the portions of monoallelic loss. RCC case numbers, which are summarized in Table I, are common to all the figures. (B) Representative result of microsatellite analyses (D6Rat8; 6q32). Arabic numbers indicate individual RCC case numbers. No preference for either allele was observed. (C) Distribution of 22 microsatellite markers and frequency of allelic loss for individual microsatellite markers are shown on the right. C, control kidney. M, magabase pairs from the telomere of the short arm of chromosome 6. LOH, loss of heterozygosity (monoallelic loss). Refer to text for details.

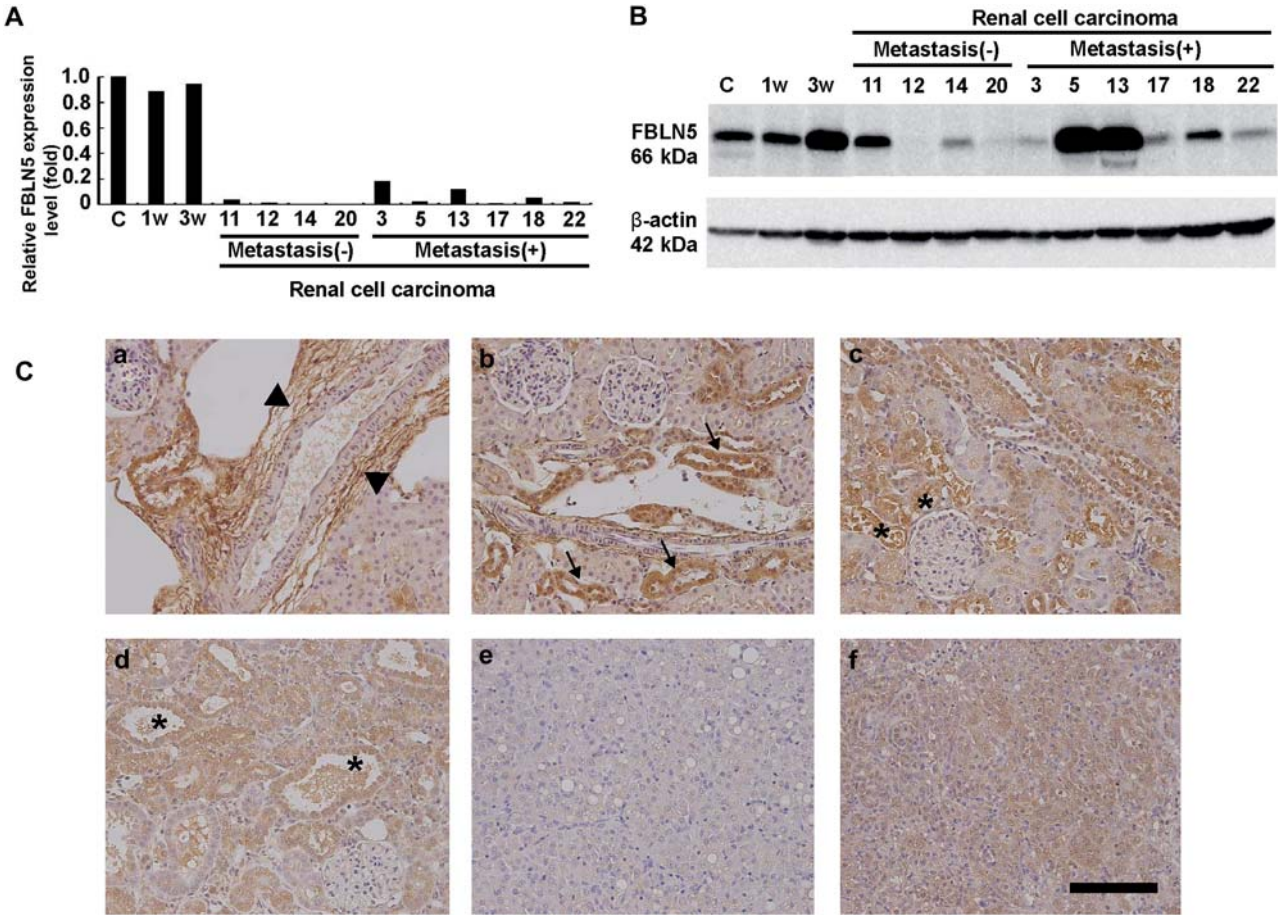

Figure 2. Message and protein analysis of the *fibulin-5* gene in the rat kidney following Fe-NTA-treatment and in the Fe-NTA-induced RCCs. (A) Expression analysis by quantitative PCR. RCCs showed low expression. 1w, 1 week; 3w, 3 weeks of sub-acute treatment. (B) Western blot analysis. After repeated Fe-NTA administration of 3 weeks, FBLN5 protein increased. Some of the RCCs with metastasis showed a prominent increase in FBLN5 protein, whereas FBLN5 level was generally low in the RCCs. Refer to text for details. (C) Immunohistochemical analysis of FBLN5. a and b, control kidney; c, kidney after 1-week treatment of Fe-NTA; d, kidney after 3-week treatment of Fe-NTA; e, RCC with no metastasis; f, RCC with pulmonary metastasis. Representative results are shown. Refer to text for details (arrowheads, immunopositivity around artery; arrows, renal distal tubules; *, renal proximal tubules; bar = 50 μm in a–f).

with an Epitect Bisulphite kit (QIAGEN) according to the manufacturer's protocol. *SssI* methyltransferase (New England Biolabs Japan Inc., Tokyo, Japan) was used for generating fully methylated DNA. PCR amplification was performed with 20 ng bisulphite-treated DNA as template in a 12.5 μl reaction mixture. Mixtures were denatured at 95°C for 5 min followed by 35 cycle of 95°C for 30 s, 58 or 60°C for 30 s and 72°C for 30 s. In the last cycle, the 72°C step was extended to 5 min. After the reaction, 5 μl of the PCR products were electrophoresed on 3% agarose gel. Primer sequences for methylated reaction were as follows: based on GenBank NC_005105; forward, 5′-GGGTTT TTAATTGTTTATATTTTTGAAGTC-3′; reverse, 5′-CGAAACGAAACGCGTACG-3′ (99 bp product, annealing temperature; 58°C). Those for the unmethylated reaction were as follows: forward, 5′-GGTTTTT AATTGTTTATATTTTTGAAGTTG-3′; reverse, 5′-CCAAAACAAAACAAAACACATACA-3′ (103 bp product, annealing temperature; 60°C).

Statistical analysis

Statistical analyses were performed with the Students's *t*-test. A $p < 0.05$ was considered statistically significant.

Results

Frequent monoallelic loss of chromosome 6 in the Fe-NTA-induced rat RCCs

We analyzed 22 Fe-NTA-induced rat RCCs and two cell lines established from these tumours, coupled with array-based comparative genomic hybridization analyses. Chromosome 6 revealed one of the highest incidences of common monoallelic loss among the 20 autosomes and X chromosome (Figure 1A). Detailed reports of the entire aCGH analyses will be published elsewhere (S Akatsuka and S Toyokuni, manuscript in preparation).

LOH on chromosome 6 reveals no allelic preference

To confirm the monoallelic loss of chromosome 6 and to evaluate whether there is any preference for either allele, LOH analyses were performed using 22 microsatellite markers spanning the major part of chromosome 6 (Figures 1B and C). We analysed 22 RCCs (Table I) including grade 1, 2 and 3 tumours (Figure 1B). LOH was detected on large areas of chromosome 6, with a range of 18.2–52.4%, which was consistent with the results of the aCGH analyses. No preference for either allele was observed, as shown in Figure 1B. Certain regions, including 6q15, exhibited a relatively higher incidence of LOH, with a frequency of more than 50% for the markers indicated in these regions (Figure 1C). The highest frequency observed was 52.4% at D6Rat28, 29 and 34, located at 6q15 (Figure 1C). We observed no significant association between the tumour grade and LOH frequency.

Expression of fibulin-5 was significantly decreased, but protein levels were variable in the Fe-NTA-induced RCCs

In combination with the data on LOH and expression microarray of 4 RCCs (Gene Expression Omnibus accession number GSE7675), we decided to focus on the *fibulin-5* gene in the present study. The expression of *fibulin-5* was not much altered after repeated administration of Fe-NTA for 1 or 3 weeks. However, it was markedly decreased in RCCs to the levels of less than 20% (Figure 2A). Fibulin-5 protein was rather increased at 3 weeks of repeated Fe-NTA administration. RCCs showed intriguing results on the proteins levels. All the RCCs with pulmonary metastasis showed recognizable western bands, with two RCCs at very high levels. Regarding RCCs without pulmonary metastasis, two showed no recognizable bands, one showed a faint band and one showed a similar density to that of the control (Figure 2B).

With immunohistochemical analyses, the control kidney showed strong positivity in the interstitial areas surrounding large vessels and in the cytoplasm of distal tubular tubules. Proximal tubules showed faint positivity. In the kidney after repeated administration of 1 or 3 weeks, immunopositivities of proximal tubules markedly increased. RCCs without metastasis showed almost no positivity, whereas some of the RCCs with metastasis showed strong cytoplasmic positivity (Figure 2C).

Expression and protein levels of fibulin-5 in cell lines

Non-transformed renal tubular cell line (NRK52E) showed high expression of *fibulin-5* with high levels of protein in its lysate. Furthermore, it was secreted to the media. In contrast, both of the RCC cell lines showed very low expression and showed no recognizable bands with western blot analysis (Figures 3A and B).

Methylation of the promoter region of fibulin-5 is partially responsible

Analyses with CpG island searcher (http://cpgislands.usc.edu/) revealed that -717 to +112 (833 bp) of rat *fibulin-5* constitute a CpG island (Figure 4A). We analysed this area with methylation-specific PCR, where analyses were possible (Figure 4B). Control kidney and NRK52E showed no methylated bands, whereas FRCC001 showed only methylated bands. FRCC562 showed both methylated and unmethylated bands. Two of the RCCs showed methylation as a major band (Figure 4C).

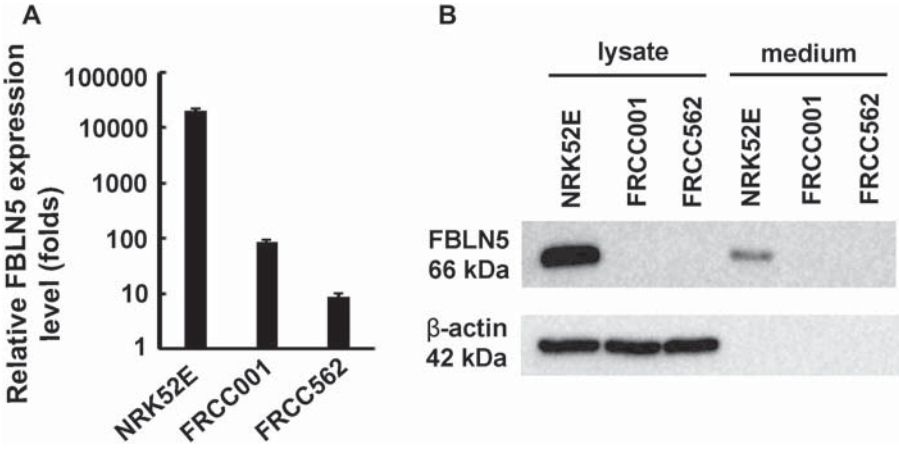

Figure 3. Analysis of *fibulin-5* in renal cell lines. (A) Expression analysis by quantitative PCR. (B) Western blot analysis of lysate and the corresponding medium. NRK52E, non-transformed renal tubular cell line; FRCC001 and FRCC562, rat RCC cell lines. Refer to text for details.

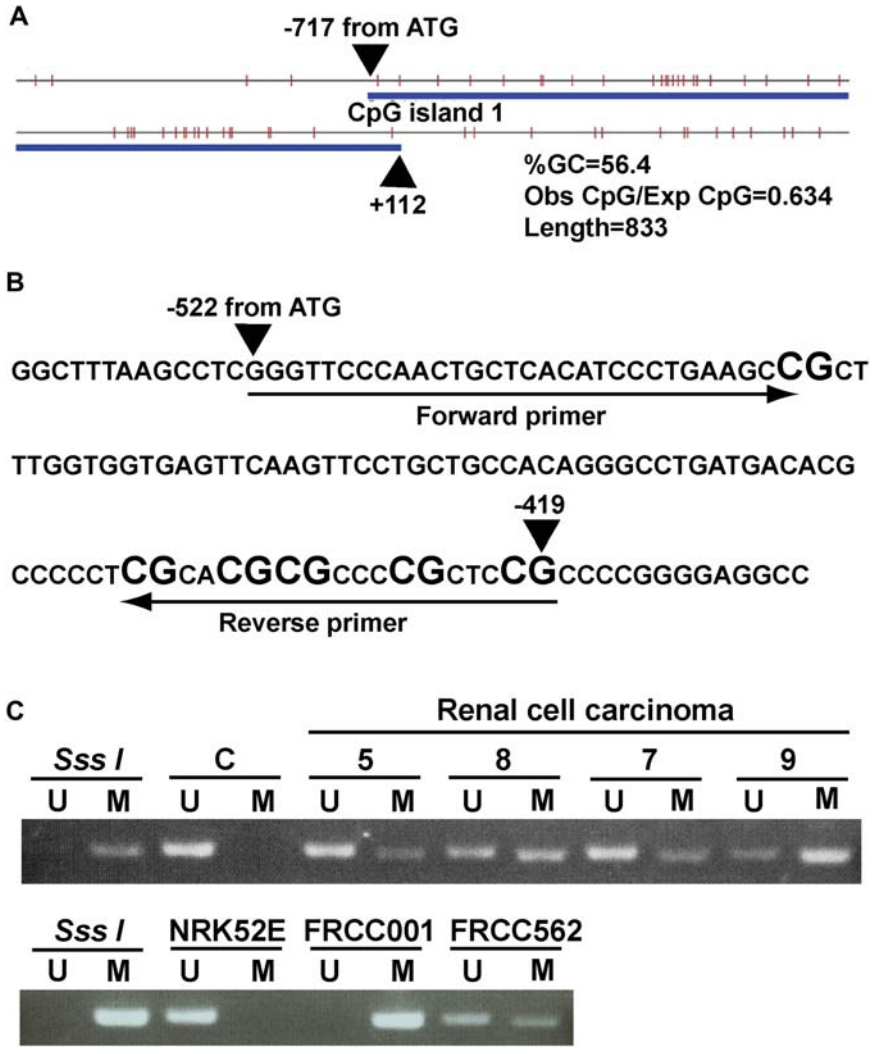

Figure 4. Methylation of the promoter region of *fibulin-5*. (A) Presence of CpG island in the promoter region. (B) Design of primers for the methylation-specific PCR analysis. (C) Methylation-specific PCR analysis. C, control kidney as negative control; U, unmethylated; M, methylated; *SssI*, treatment of genomic DNA for full methylation as positive control. Refer to text for details.

Neither proliferation, migration nor invasion was associated with the fibulin-5 gene in the cell line experiments

Two rat RCC cell lines that practically show no FBLN5 protein (Figure 3B) were stably transfected with *fibulin-5* and proliferation, migration and invasion were evaluated, using cells with an empty vector as a control. We did not find the statistically significant difference for all the three factors (data not shown).

Myofibroblasts in the primary tumor of RCCs

To obtain insights into the increased *fibulin-5* protein in some of the RCCs with pulmonary metastasis, we studied the localization of myofibroblasts in the primary lesion of RCCs because myofibroblasts have been associated with metastasis [33]. We used α-smooth muscle actin as a marker of myofibroblasts. In addition to the higher levels of *fubulin-5* immunopositivity in the RCCs with metastasis, we observed proliferation of myofibroblasts intermingled with cancer cells only in the RCCs with metastasis (Figure 5).

Discussion

The Fe-NTA-induced RCC model offers a superb opportunity to elucidate the molecular mechanisms of oxidative stress-induced cancer [4]. Furthermore, this model presents a prominent similarity to its human counterpart. Namely, more than half of the RCC cases metastasize to the lung that ultimately kills the animal [8]. We have selected the *fibulin-5* gene, based on the data of expression microarray, aCGH as well as microsatellite analyses. FBLN5 protein is associated with elastic fibre formation as a Ca^{2+}-dependent elastin binding protein [19,20], so it was present in the interstitial tissue surrounding large vessels in the normal kidney. In such a situation, we have to be careful not to pick up just the population effects

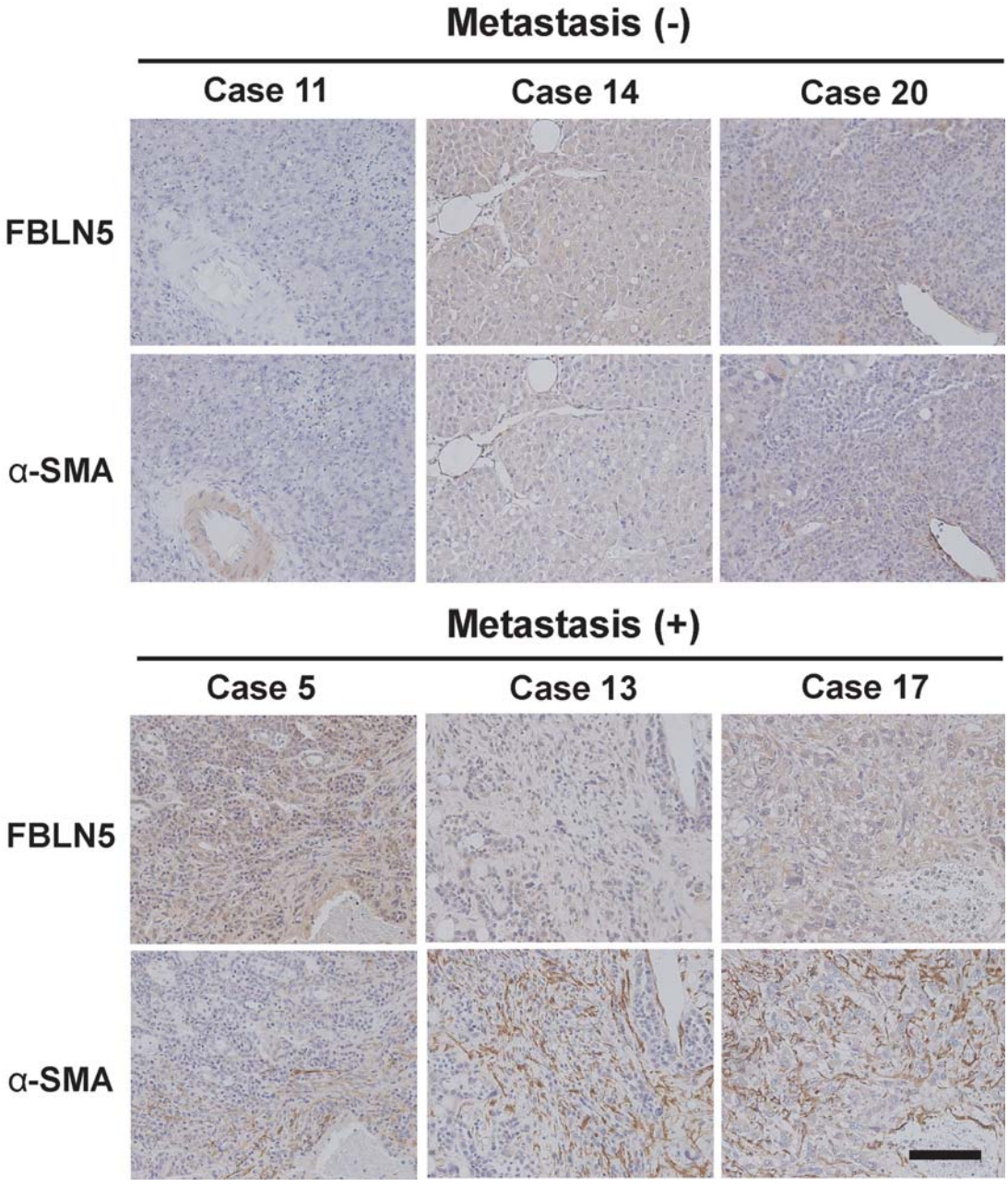

Figure 5. Association of FBLN5 and α-smooth muscle actin (α-SMA) in the Fe-NTA-induced RCCs exhibiting pulmonary metastasis with immunohistochemical analysis. All the immunohistochemical analysies are paired with serial section techniques of the paraffin embedded specimens. Representative results are shown. Non-neoplastic large vessels contain smooth muscle, thus working as a positive control for α-SMA. Note that case numbers correspond to those in Table I and other figures. Refer to text for details (bar = 50 μm).

because large vessels are not usually present in the tumour samples. To completely rule out this kind of problem in the gene screening process, a laser microdissection technique would be helpful. However, bulk screening such as this case is also useful only if careful consideration and studies are conducted and is even advantageous in that the interaction between epithelial and interstitial cells is not neglected.

As far as we know, not much data is available on the localization of FBLN-5 protein in the kidney. We found that they are also present in the renal tubules, especially distal tubules. We performed laser microdissection and confirmed the presence of *fbln5* message in the tubular cells (H Ohara and S Toyokuni, unpublished data). The main function of renal tubules is the reabsorption of precious biomolecules such as sugar, amino acids and water, so every renal tubule is escorted by small and thin vessels. Thus, FBLN-5 here may work as an endogenous angiogenesis inhibitor [26]. Production and secretion of FBLN5 was confirmed by cell culture experiments using NRK52E (Figure 3B).

Oxidative stress is associated with chronic inflammation bidirectionally. Chronic interstitial inflammation is observed in the kidney in this carcinogenesis model

[34]. Here prominent increase in FBLN5 was observed in the renal tubules 1–3 weeks after repeated oxidative stress by Fe-NTA (Figure 2). As a molecular mechanism of FBLN5 increase, a decrease in proteolysis appears to play a role since message level is not different between the control and the 3-week. It is possible that FBLN5 exerts a feedback mechanism to decrease angiogenesis as described above [26]. We have done an experiment by the use of *fbln5* knockout mice [19] to see the difference in the proliferation of renal tubular cells after repeated administration of Fe-NTA. We found that proliferation as seen by immunoreactivity for proliferating cell nuclear antigens was higher in the knockout mice than the wild-type, but this was not statistically significant ($p = 0.10$) (H Ohara and S Toyokuni, unpublished data).

In the RCCs, the message levels of *fibulin-5* were all low (Figure 2A). However, the protein levels were quite different among tumours (Figure 2B). We searched for the methylation of the promoter region of this gene. In the FRCC001 cell line, it was clear that *fibulin-5* was shut down by this mechanism (Figure 4C), but the results for the RCCs were not easy to interpret. We think that methylation of the promoter region partially explains the low message, but other mechanisms such as transcription factor and miRNA have to be considered in future experiments.

By careful observation we found that RCCs with metastasis always show recognizable bands for FBLN5 protein with western blot analysis, with some tumours harbouring prominent amounts of the protein. The discrepancy between the message and protein levels again suggests a molecular mechanism at the proteolytic level. Probably, specific proteolytic machinery such as ubiquitin ligase is suppressed in these tumours, which is currently under investigation. To link FBLN5 and metastasis, we undertook to identify myofibroblasts in the tumours, which are thought to be associated with metastasis. Myofibroblast is a kind of fibroblast that has acquired tactile migration activity with the help of cytoplasmic α-smooth muscle actin [33]. Recently, it was reported that oxidative stress promotes myofibroblast differentiation [35]. It was intriguing to find that high levels of FBLN5 protein in the RCCs and myofibroblasts were closely associated in our model (Figure 5). This suggests that FBLN5 secreted by tumour cells may work as a cytokine to transform interstitial cells such as fibroblast to myofibroblast or to accumulate myofibroblasts. Whether this hypothesis is correct or not requires further investigation. If so, FBLN-5-blocking antibodies may be effective in combating tumour metastasis in specific cancers like this model. We do not deny that other mechanisms are also in operation for metastasis. It was interesting to note here that FBLN5 was not observed in the surrounding area of large vessels in the RCCs without metastasis (Figure 5, case 11); suggesting that some suppression mechanisms are working presumably from the non-metastasizing tumours.

We focused on the *fibulin-5* gene after the genome-wide screening. Loss of heterozygosity was found in about half of the cases but no homozygous deletion was observed for this gene (Figure 1). This is probably associated with the fact that the tumour requires this gene at a late stage for metastasis, thus the clones with homozygous deletion did not remain. In the RCCs without metastasis, FBLN5 was in a low level. However, RCCs with pulmonary metastasis mostly presented high levels of FBLN5 associated with myofibroblast proliferation. This gene was associated neither with the proliferation, migration nor invasion of transformed cells at least in this model. In conclusion, FBLN5 play stage-specific roles in oxidative stress-induced renal carcinogenesis and our results suggest that it works as a cytokine regulated by post-translational mechanisms.

Declaration of interest

This work was supported in part by a MEXT grant (Special Coordination Funds for Promoting Science and Technology), a Grant-in-Aid from the Ministry of Education, Culture, Sports, Science and Technology of Japan, a Grant-in-Aid for Cancer Research from the Ministry of Health, Labour and Welfare of Japan, and a grant from Takeda Science Foundation.

References

[1] Halliwell B, Gutteridge JMC. Free radicals in biology and medicine. Oxford: Oxford University Press; 2007.
[2] Toyokuni S. Iron-induced carcinogenesis: the role of redox regulation. Free Radic Biol Med 1996;20:553–566.
[3] Valko M, Rhodes C, Moncol J, Izakovic M, Mazur M. Free radicals, metals and antioxidants in oxidative stress-induced cancer. Chem Biol Interact 2006;160:1–40.
[4] Toyokuni S. Molecular mechanisms of oxidative stress-induced carcinogenesis: from epidemiology to oxygenomics. IUBMB Life 2008;60:441–447.
[5] Toyokuni S. Role of iron in carcinogenesis: cancer as a ferrotoxic disease. Cancer Sci 2009;100:9–16.
[6] Ebina Y, Okada S, Hamazaki S, Ogino F, Li JL, Midorikawa O. Nephrotoxicity and renal cell carcinoma after use of iron- and aluminum- nitrilotriacetate complexes in rats. J Natl Cancer Inst 1986;76:107–113.
[7] Li JL, Okada S, Hamazaki S, Ebina Y, Midorikawa O. Subacute nephrotoxicity and induction of renal cell carcinoma in mice treated with ferric nitrilotriacetate. Cancer Res 1987;47:1867–1869.
[8] Nishiyama Y, Suwa H, Okamoto K, Fukumoto M, Hiai H, Toyokuni S. Low incidence of point mutations in H-, K- and N-ras oncogenes and p53 tumor suppressor gene in renal cell carcinoma and peritoneal mesothelioma of Wistar rats induced by ferric nitrilotriacetate. Jpn J Cancer Res 1995;86:1150–1158.
[9] Toyokuni S, Mori T, Dizdaroglu M. DNA base modifications in renal chromatin of Wistar rats treated with a renal carcinogen, ferric nitrilotriacetate. Int J Cancer 1994;57:123–128.
[10] Toyokuni S, Luo XP, Tanaka T, Uchida K, Hiai H, Lehotay DC. Induction of a wide range of C_{2-12} aldehydes and C_{7-12} acyloins in the kidney of Wistar rats after treatment with a

renal carcinogen, ferric nitrilotriacetate. Free Radic Biol Med 1997;22:1019–1027.
[11] Toyokuni S, Uchida K, Okamoto K, Hattori-Nakakuki Y, Hiai H, Stadtman ER. Formation of 4-hydroxy-2-nonenal-modified proteins in the renal proximal tubules of rats treated with a renal carcinogen, ferric nitrilotriacetate. Proc Natl Acad Sci USA 1994;91:2616–2620.
[12] Jiang L, Zhong Y, Akatsuka S, Liu Y, Dutta K, Lee W, Onuki J, Masumura K, Nohmi T, Toyokuni S. Deletion and single nucleotide substitution at G:C in the kidney of gpt delta transgenic mice after ferric nitrilotriacetate treatment. Cancer Sci 2006;97:1159–1167.
[13] Tanaka T, Iwasa Y, Kondo S, Hiai H, Toyokuni S. High incidence of allelic loss on chromosome 5 and inactivation of p15 ^{INK4B} and p16 ^{INK4A} tumor suppressor genes in oxystress-induced renal cell carcinoma of rats. Oncogene 1999;18: 3793–3797.
[14] Hiroyasu M, Ozeki M, Kohda H, Echizenya M, Tanaka T, Hiai H, Toyokuni S. Specific allelic loss of p16^{INK4A} tumor suppressor gene after weeks of iron-mediated oxidative damage during rat renal carcinogenesis. Am J Pathol 2002;160: 419–424.
[15] Liu Y-T, Shang D-G, Akatsuka S, Ohara H, Dutta KK, Mizushima K, Naito Y, Yoshikawa T, Izumiya M, Abe K, Nakagama H, Noguchi N, Toyokuni S. Chronic oxidative stress causes amplification and overexpresson of ptprz1 protein tyrosine phosphatase to activate β-catenin pathway. Am J Pathol 2007;171:1978–1988.
[16] Tanaka T, Akatsuka S, Ozeki M, Shirase T, Hiai H, Toyokuni S. Redox regulation of annexin 2 and its implications for oxidative stess-induced renal carcinogenesis and metastasis. Oncogene 2004;23:3980–3989.
[17] Zacharski L, Chow B, Howes P, Shamayeva G, Baron J, Dalman R, Malenka D, Ozaki C, Levori P. Decreased cancer risk after iron reduction in patients with peripheral arterial disease: results from a randomized trial. J Natl Cancer Inst 2008;100:996–1002.
[18] Nakamura T, Ruiz-Lozano P, Lindner V, Yabe D, Taniwaki M, Furukawa Y, Kobuke K, Tashiro K, Lu Z, Andon NL, Schaub R, Matsumori A, Sasayama S, Chien KR, Honjo T. DANCE, a novel secreted RGD protein expressed in developing, atherosclerotic, and balloon-injured arteries. J Biol Chem 1999;274:22476–22483.
[19] Nakamura T, Lozano PR, Ikeda Y, Iwanaga Y, Hinek A, Minamisawa S, Cheng CF, Kobuke K, Dalton N, Takada Y, Tashiro K, Ross J, Jr, Honjo T, Chien KR. Fibulin-5/DANCE is essential for elastogenesis *in vivo*. Nature 2002;415:171–175.
[20] Yanagisawa H, Davis EC, Starcher BC, Ouchi T, Yanagisawa M, Richardson JA, Olson EN. Fibulin-5 is an elastin-binding protein essential for elastic fibre development *in vivo*. Nature 2002;415:168–171.
[21] Markova D, Zou Y, Ringpfeil F, Sasaki T, Kostka G, Timpl R, Uitto J, Chu ML. Genetic heterogeneity of cutis laxa: a heterozygous tandem duplication within the fibulin-5 (FBLN5) gene. Am J Hum Genet 2003;72:998–1004.
[22] Stone EM, Braun TA, Russell SR, Kuehn MH, Lotery AJ, Moore PA, Eastman CG, Casavant TL, Sheffield VC. Missense variations in the fibulin 5 gene and age-related macular degeneration. N Engl J Med 2004;351:346–353.
[23] Albig AR, Schiemann WP. Fibulin-5 function during tumorigenesis. Future Oncol 2005;1:23–35.
[24] Schiemann WP, Blobe GC, Kalume DE, Pandey A, Lodish HF. Context-specific effects of fibulin-5 (DANCE/EVEC) on cell proliferation, motility, and invasion. Fibulin-5 is induced by transforming growth factor-beta and affects protein kinase cascades. J Biol Chem 2002;277:27367–27377.
[25] Yue W, Sun Q, Landreneau R, Wu C, Siegfried JM, Yu J, Zhang L. Fibulin-5 suppresses lung cancer invasion by inhibiting matrix metalloproteinase-7 expression. Cancer Res 2009;69:6339–6346.
[26] Sullivan KM, Bissonnette R, Yanagisawa H, Hussain SN, Davis EC. Fibulin-5 functions as an endogenous angiogenesis inhibitor. Lab Invest 2007;87:818–827.
[27] Lee YH, Albig AR, Regner M, Schiemann BJ, Schiemann WP. Fibulin-5 initiates epithelial-mesenchymal transition (EMT) and enhances EMT induced by TGF-beta in mammary epithelial cells via a MMP-dependent mechanism. Carcinogenesis 2008;29:2243–2251.
[28] Zhong Y, Onuki J, Yamasaki T, Ogawa O, Akatsuka S, Toyokuni S. Genome-wide analysis identifies a tumor suppressor role for aminoacylase 1 in iron-induced rat renal cell carcinoma. Carcinogenesis 2009;30:158–164.
[29] Toyokuni S, Kawaguchi W, Akatsuka S, Hiroyasu M, Hiai H. Intermittent microwave irradiation facilitates antigen-antibody reaction in Western blot analysis. Pathol Int 2003;53:259–261.
[30] Hirai M, Ohbayashi T, Horiguchi M, Okawa K, Hagiwara A, Chien KR, Kita T, Nakamura T. Fibulin-5/DANCE has an elastogenic organizer activity that is abrogated by proteolytic cleavage *in vivo*. J Cell Biol 2007;176:1061–1071.
[31] Hirai M, Horiguchi M, Ohbayashi T, Kita T, Chien KR, Nakamura T. Latent TGF-beta-binding protein 2 binds to DANCE/fibulin-5 and regulates elastic fiber assembly. EMBO J 2007;26:3283–3295.
[32] Goldman L, Cutrone E, Kotenko S, Krause C, Langer J. Modifications of vectors pEF-BOS, pcDNA1 and pcDNA3 result in improved convenience and expression. Biotechniques 1996;21:1013–1015.
[33] Grunert S, Jechlinger M, Beug H. Diverse cellular and molecular mechanisms contribute to epithelial plasticity and metastasis. Nat Rev Mol Cell Biol 2003;4:657–665.
[34] Nishiyama Y, Tanaka T, Naitoh H, Mori C, Fukumoto M, Hiai H, Toyokuni S. Overexpression of integrin-associated protein (CD47) in rat kidney treated with a renal carcinogen, ferric nitrilotriacetate. Jpn J Cancer Res 1997;88:120–128.
[35] Toullec A, Gerald D, Despouy G, Bourachot B, Cardon M, Lefort S, Richardson M, Rigaill G, Parrini MC, Lucchesi C, Bellanger D, Stern MH, Dubois T, Sastre-Garau X, Delattre O, Vincent-Salomon A, Mechta-Grigoriou F. Oxidative stress promotes myofibroblast differentiation and tumour spreading. EMBO Mol Med 2010;2:211–230.

This paper was first published online on Early Online on 4 October 2010.